AIAA Guidance, Navigation and Control Conference and Exhibit
20 - 23 August 2007, Hilton Head, South Carolina

AIAA 2007-6514

Nonlinearity in Sensor Fusion: Divergence Issues in EKF, modified truncated SOF, and UKF

L. Perea* J. How† L. Breger† P. Elosegui*

Relative navigation is a challenging technological component of many planned NASA and ESA missions. It typically uses recursive filters to fuse measurements (e.g., range and angle) from sensors with contrasting accuracies to estimate the vehicle state vectors in real time. The tendency of Extended Kalman filter to diverge under these conditions is well documented in the literature. As such, we have investigated the application of the modified truncated Second-Order Filter (mtSOF) and the Unscented Kalman filter (UKF) to those mission scenarios using numerical simulations of a representative experimental configuration: estimation of a static position in space using distance and angle measurements. These simulation results showed that the mtSOF and UKF may also converge to an incorrect state estimate. A detailed study establishes the divergence process of the mtSOF and UKF, and designs new strategies that improve the accuracy of these filters.

I. Introduction

Formation flying is expected to become a core technology component of future space missions such as Symbol-X, TPF, and DARWIN. Missions demonstrating formation flying technologies, e.g. the Proba 3 concept[1] of the European Space Agency (ESA), are under consideration at space agencies worldwide. These missions may combine measurements from various sensors,[2] likely with different accuracies, to meet position and attitude requirements defined both for the individual satellites and for the formation. Measurements such as range and bearing will require nonlinear estimators that are robust and can also operate autonomously for extended periods of time.[3] This study investigates divergence properties of high-order filters, in particular the unscented Kalman filter (UKF), in the presence of nonlinearities; and evaluates proposed modifications to improve filter performance.

The extended Kalman filter (EKF) is a nonlinear filter that is used extensively because it usually provides very good estimation performance and has a straightforward implementation. However, the EKF has been shown to fail (i.e., to diverge or to converge to an incorrect solution) in many object tracking applications where the dynamic models, measurement models, or both, are not linear functions of the state vector.[4,5] An example of this is determining the orbit of a satellite formation using Global Positioning System (GPS) measurements and inter-vehicle ranging (e.g., using microwave signals), for which EKF has been shown to be unreliable.[6] Huxel et al. characterized the error associated with the EKF and the modified Gaussian second-order filter due to the combination of inertial and relative range measurements with different accuracies. Plinval[7] and Mandic[8] further analyzed the divergence process of the EKF under similar conditions, and investigated the performance of an alternative recursive filter focusing on an *ad hoc* increase of the measurement noise levels,[7–10] a technique also known as "Bump-up."

There are several other filters in the literature that have been designed to deal with nonlinear measurements,[5–7,11–18] with respect to the state vector. These filters use different approximations of the measurement models, different approximations of the probability density functions, or both. For example, there exists a large set of filters that are variations of the EKF. The iterated EKF (IEKF) is known for its accuracy with nonlinear measurement models conditioned to ensure that the system is fully observable.[14] Its main drawback is the computational load associated with the additional filter iterations that are required. The linear regression Kalman filters (LRKF) represent another set of variants that approximate the state/measurement estimate and the associated uncertainty by a statistical linear regression through a well chosen set of "sigma

*Institute for Space Sciences, CSIC–IEEC, Barcelona, Spain
†Department of Aeronautics and Astronautics, MIT, Cambridge, MA, USA

points". This process allows multiple moments of the probability density function and terms of the Taylor series expansion of the dynamic/measurement models to be considered. Some examples of this family are the central difference filter, the first-order divided difference filter, and the recent unscented Kalman filter (UKF).[13,14,19] These filters require the evaluation of the measurement model at several points, but, in contrast with the EKF and IEKF, they avoid the computation of the Jacobian of the models. This makes them particularly well suited to the case where the evaluation of the Jacobian is complex or computationally expensive.

Another important set of filters are the high-order filters. The second-order filters (SOF) are probably the best known among them. These filters approximate the models by a high-order Taylor approximation, and assume that the third and higher-order moments of the probability functions are a function of the covariance.[15] The complexity and computational load required for the implementation of these types of filters typically make their implementation unfeasible, particularly in the vector case ($x \in \mathbb{R}^n, \quad n > 1$).[15] In the case of the SOF family, some simplifications have been designed to avoid the complexity of implementing a full SOF. For example, the mtSOF, which accounts for bias correction terms due to nonlinearities in the models,[15] is commonly used.

Particle filters approximate the full probability distribution, not only the mean and the variance, by using a finite set of samples. These filters use the sequential sampling and resampling according to an "importance function" to provide much better performance than Kalman filters. The improved performance is especially pronounced when using nonlinear models (e.g., object tracking using bearing sensors[5]), or non-Gaussian distributions. However, the high computational cost associated with using the large number of samples required makes them unsuitable for almost real-time navigation applications.[5,12]

This study is aimed at characterizing the error due to nonlinear measurements (with respect to the state vector) using different kinds of filters suitable for near real-time missions, such as those presented above. For this purpose, we evaluated the estimation performance of a representative set of filters: the EKF,[4,9,15] bump-up strategies based on the EKF,[6–10] the mtSOF,[15] and the UKF.[5,13] We used a popular experimental case[5,7,8] that allows full isolation of the performance of the update equations from the propagation equations. We evaluated the estimation performance and long-time stability of these filters under identical experimental conditions, and designed possible modifications to improve their performance, when possible.

In the following sections, we introduce previous filters using a unified approach for describing both prediction and update phases. This notation permits straightforward comparisons between filters and makes clear the respective roles of each term in the filter equations. Because of their common structure we will refer to this kind of filters as Kalman-type filters in the sequel. The errors and divergence processes of these Kalman-type filters are characterized in detail. Then, proposed modifications to these filters are described that improve their performance in the presence of nonlinear measurement models. These modifications have been evaluated for a large set of experimental configurations.

II. Description of Kalman-type filters

The extended Kalman filter, the *modified truncated* second-order filter, and the unscented Kalman filter all belong to a common family of Kalman-type filters. They are used to estimate the n-dimensional state $x \in \mathbb{R}^n$ of a process that is governed by an *almost-linear* stochastic differential equation,

$$\dot{x} = f(t, x)dt + G(t, x)d\beta(t)$$

through the measurements $z \in \mathbb{R}^m$

$$z = h(x) + v$$

where $\dot{x}$ is the time derivative of the state vector x, n is the dimension of x, f is the dynamic model function, t is time, G is an n-by-s function, β is an s-vector dimensional Brownian motion of diffusion $Q(t)$, z is the measurement vector, m is the dimension of z, h is the measurement modeling function, and v is the measurement noise ($\sim N(0, R)$). The state estimation procedure has two distinct phases: first, it predicts the statistics that describe the distribution of the state x at time $t - \Delta t$ to time t, when new measurements will be available; and second, it updates the predicted state estimate as new measurements become available.

Kalman-type filters are based on the assumption that the state, measurement, and error distributions can be characterized by only two statistics: the mean and the covariance. Higher order central moments are assumed small enough to be neglected. Therefore, the equations used to propagate and update the state

estimates are based on different approximations of the following conditional expectations

$$\hat{x}_k^- = E[x(t_k)|z(t_{k-1}) = z_{k-1}] \quad (1)$$

$$P_{xx,k}^- = E[(x(t_k) - \hat{x}_k^-)(x(t_k) - \hat{x}_k^-)^T|z(t_{k-1}) = z_{k-1}] \quad (2)$$

$$\hat{x}_k^+ = E[x(t_k)|z(t_k) = z_k] \quad (3)$$

$$P_{xx,k}^+ = E[(x(t_k) - \hat{x}_k^+)(x(t_k) - \hat{x}_k^+)^T|z(t_k) = z_k] \quad (4)$$

where the character $\hat{}$ denotes estimated value, k is a time index, $^-$ indicates a predicted value, $z(t)$ is the measurement variable, z_k is the measurement, $P_{xx,k}$ is the covariance matrix of the state estimate, ^{T} denotes matrix transpose, and $^+$ indicates an updated term.

The approximations of the conditional expectations (1) and (2) corresponding to the prediction phase are called prediction equations, and they vary between filters. The EKF propagates the state estimate statistics (i.e., the mean and the covariance) by integrating the linearized differential equations. Therefore, the statistics estimated using the EKF are linear approximations of the true mean and true covariance matrix. On the other hand, the mtSOF and UKF may propagate the state statistics using higher-order terms of the nonlinear dynamic model f, thus increasing their accuracy with respect to the EKF. In particular, the mtSOF includes second-order terms of the dynamic model by using the first and second derivatives of f, thereby increasing the complexity of the algorithm implementation in many problems.[15] The UKF circumvents such increased complexity by generating a set of well distributed points around the current estimate, propagating this set of sigma points to the next epoch, and then re-computing the statistics from the resulting set of sigma points. Depending on the number and distribution of the original sigma points, the UKF can include high-order terms of the dynamic model f with adjustable accuracy for these equations, though this can also add complexity in the selection of the sigma points.[12]

To approximate the conditional expectations (3) and (4) of the update phase, all previous filters use the following approximations, which are usually referred to as update equations:

$$K_k = P_{xz,k}P_{zz,k}^{-1} \quad (5)$$

$$\hat{x}_k^+ = \hat{x}_k^- + K_k(z_k - \hat{z}_k) \quad (6)$$

$$P_{xx,k}^+ = P_{xx,k}^- - P_{xz,k}(P_{zz,k})^{-1}P_{xz,k}^T \quad (7)$$

where K_k is the Kalman gain matrix, P_{xz} is the covariance matrix between the state and the measurement, P_{zz} is the covariance matrix of the measurements, z is a vector of measurements, $\hat{z}$ are the expected measurements, and $(z_k - \hat{z}_k)$ are the innovations or measurement residuals.

Equations (5) - (7) correspond to a linear function of the measurement residuals, and that the coefficients are functions of $\hat{x}_k^-$, P_k^-, and h. When h is a nonlinear function, the coefficients are also nonlinear functions of the state space statistics and each filter generally computes them with the same degree of accuracy as that used in the propagation equations. For the computation of $\hat{z}_k$, P_{zz}, and P_{xz}, the state statistics $\hat{x}_k^-$ and P_k^- are transformed to the measurement space using the same approximations of (1) and (2). The EKF transforms mean and covariance using a linearization of the measurement function h; the mtSOF transforms these statistics using the first and second derivatives of h; the UKF generates a set of sigma points for this transformation.

Figure 1 shows the performance of these filters for the case of a static vehicle (i.e., $f(t, x) = 0$) in $\mathbb{R}^2$ without process noise ($Q(t) = 0$), using linear measurements (e.g., $h(x) = x$), and independent measurement noise levels (R is diagonal, with elements $\sigma_1 = 2.5\text{E}{-5}$ and $\sigma_2 = 6\text{E}{-3}$ in the example shown). Under this configuration, both the EKF and the mtSOF coincide because there are no second-order terms, and all three filters provide good estimates from the first iteration, as expected for linear measurements. The following sections analyze the suitability of the linear assumptions of the update equations in the EKF, mtSOF, and UKF in experimental configurations that involve highly nonlinear measurements.

III. Description of the experimental configuration

In order to address the accuracy of the update equations, we will consider the estimation of a fixed position in Cartesian coordinates $x = (x_1, x_2)$ in $\mathbb{R}^2$ (i.e., a system with no dynamics $\dot{x} = f(t, x) = 0$ and $Q \equiv 0$ as in Figure 1), thus effectively isolating the prediction phase from the update phase. The nonlinear measurements considered are distance $r = \sqrt{x_1^2 + x_2^2}$ and angle $\theta = \arctan(x_2/x_1)$. This configuration

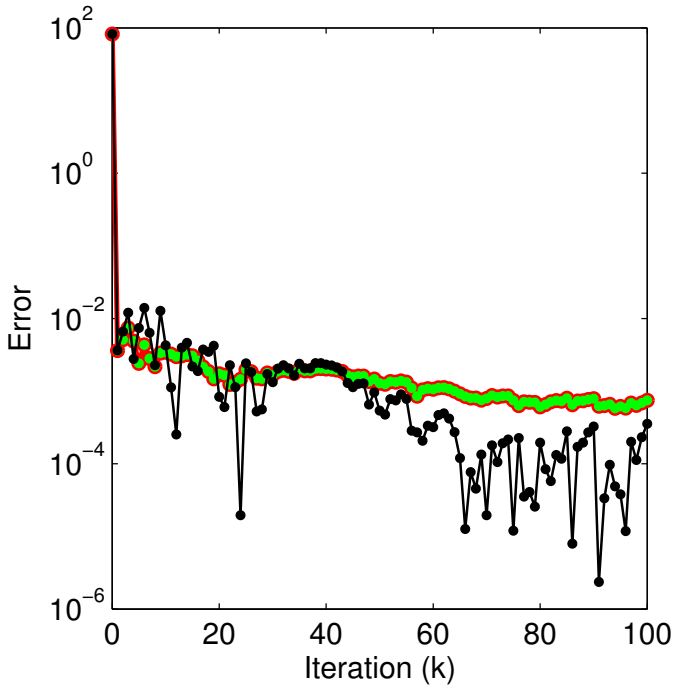

Figure 1. Variation of the (red) EKF, (green) mtSOF, and (black) UKF position error of a static vehicle using linear measurements. Note that the vertical axis is in logarithmic scale.

was previously employed by several authors[5,7,8] to evaluate the performance of the EKF. It is particularly well-suited for filter evaluation because of its simplicity and nonlinearity.

The propagation equations associated with this problem are identical for all filters:

$$\hat{x}_k^- = \hat{x}_{k-1}^+ \tag{8}$$

$$P_{xx,k}^- = P_{xx,k-1}^+ \tag{9}$$

We have chosen to make the distance measurements significantly more accurate than the angle measurements to be representative of sensor suites on possible future proposed formation flying missions.[7,8,20] As a baseline configuration $\tilde{x}_{true} = (100, 100)$ units; the covariance matrix of measurement noise R is a diagonal matrix with a radial measurement noise level σ_r^2 of 2.5E−5 square units, and an angular noise level σ_θ^2 of 6E−3 square radians; an a priori state estimate $\hat{x}_0 = (20, 80)$; and the a priori state uncertainty $P_{xx,0} = \sigma^2 I$, where $\sigma = 100$. Other values will be used in the sensitivity analysis (see below). Perfect measurements have been used as realizations of the measurement variable z, i.e., $z(t_k) = h(\tilde{x}_{true})$ for every k. This represents a best-case scenario in which measurements are better-than-expected under normal experimental conditions.

IV. Divergence process of the EKF

To introduce the problem of filter divergence, an analysis of the EKF divergence process is presented first. The explicit expressions for the coefficients of the update equations (6)–(7) in the EKF are:

$$\hat{z}_k = h(\hat{x}_k^-) \tag{10}$$

$$P_{zz,k} = R + H_k P_{xx,k}^- H_k^T \tag{11}$$

$$P_{xz,k} = P_{xx,k}^- H_k^T \tag{12}$$

where $H_k = \frac{\partial h}{\partial x}\big|_{\hat{x}_k^-}$ is the Jacobian matrix of $h(x)$ evaluated at $x = \hat{x}_k^-$.

The EKF linearizes the nonlinear measurement function h around the current predicted state estimate and ignores higher-order terms. Although widely used, the EKF is thus only reliable for systems that are almost linear within the time scale of the update interval.[19] Plinval[7] and Mandic[8] evaluated the performance

of this filter for the problem described in Section III and found that it failed to converge to the true position regardless of the number of filter iterations, a process that they diagnosed as filter divergence. They determined that the divergence was due to an over-reduction of the state covariance matrix in all dimensions, which, in turn, was caused by the nonlinearities of the measurement model. They found that the true state vector lies outside the ellipsoid that approximates the confidence area of the estimated state vector after a few filter iterations. This section builds on that example to further investigate the problem of filter divergence.

Figure 2(a) shows the experimental configuration after the first filter iteration. The estimation process starts with the initial state estimate at the (unitless) position $\hat{x}_0^+ = (20, 80)$, and the true position $\tilde{x}_{true} = (100, 100)$. During the first measurement update, the radial component of the measurement residual is projected into the direction of $\hat{x}_1^- = \hat{x}_0$ from the origin of coordinates -this direction will be referred to as radial direction in the sequel-, and the angular component of the measurement residual is projected onto its tangential direction due to the linearization process of the measurement model. Due to the linear model of the measurement update equations, both contributions are combined through simple addition, leading to the new state estimate $\hat{x}_1^+ = (77.36, 126.43)$. The resulting error in the update state estimate $\tilde{x}_{true} - \hat{x}_1^+$ is significantly large compared to the measurement noise R.

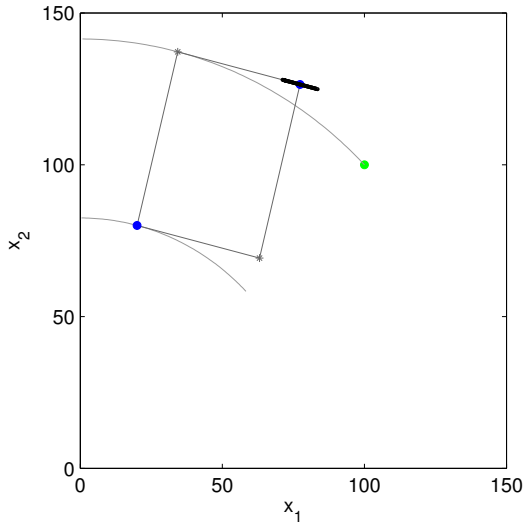

(a) First update process. This figure depicts (green) $\tilde{x}_{true} = (100, 100)$, (blue) $\hat{x}_1^- = \hat{x}_0 = (20 \quad 80)$, (grey) the new state variation due to the radial residual (along the radial direction), and to the angular residual (along the linearized angular direction), (blue) the resulting update state estimate $\hat{x}_1^+ = (77.36 \quad 126.43)$, and (black) the 1-$\sigma^2$ confidence area associated to the state covariance matrix $P_{xx,1}^+$. Note that the ellipse $P_{xx,1}^+$ has almost collapsed to an interval.

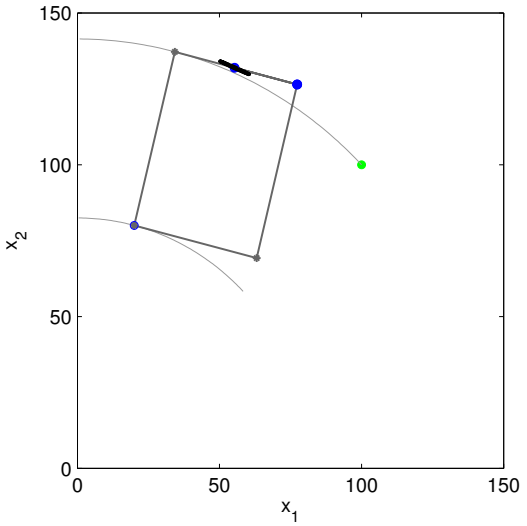

(b) Second update process. This figure depicts $\hat{x}_1^- = \hat{x}_0$, $x_2^- = x_1^+$, the new state variation due to the radial residual (along the linearized angular direction of $\hat{x}_0$ due to the erroneous correlation of $P_{zz,2}$), and to the angular residual (undetectable due to its small size), $\hat{x}_2^+ = (55.32 \quad 131.94)$. The resulting (black) 1-σ^2 confidence area associated to the state covariance matrix $P_{xx,2}^+$ has contracted so much that it can not be appreciated in this picture, for this reason we plotted 10^4-σ^2 confidence area.

Figure 2. EKF update process.

The state covariance update remains unaffected by the error in the state update because the former assumes a linear measurement model. The magnitude of the update state covariance is greatly reduced in all directions due to the small size of the measurement noise levels (R matrix). Due to the differences in the measurement noise levels, the confidence area has contracted faster in the direction of $\hat{x}_1^- = \hat{x}_0$ than in the linearized angular direction. The confidence area of the new state estimate corresponds to an ellipsoid with axis parallel to the eigenvectors of $P_{xx,1}^+$, that correspond to the radial and angular directions of $\hat{x}_1^- \neq x_1^+$. Figure 2(a) shows that the large reduction of the state covariance has allowed the solution $\tilde{x}_{true}$ to fall outside the 1-σ confidence area defined by $P_{xx,1}^+$.

After the first update, the radial and angular directions associated with the new state $\hat{x}_1^+$ have changed. Therefore, the eigenvectors of $P_{xx,1}^+$ do not correspond to the radial and angular directions of $\hat{x}_1^+$. This misalignment, together with the high condition number of the state covariance, result in a significant term appearing in the off-diagonal of $P_{zz,2} = (R + H_k P_{xx,2}^- H_k^T)^{-1}$. The presence of this term is interpreted by the

filter as indicating a correlation between the radial and the angular measurements, which leads the filter to a misinterpretation of the residuals during the next update. Figure 2(b) shows that the new measurement residuals are further misinterpreted leading to an update state estimate with a larger error than the first update. Since the covariance matrix update is independent of the residuals, the updated covariance matrix shrinks again in all directions ($P^{+}_{xx,1}$ has been magnified by 10^4 in Figure 2(b); see figure caption).

At this stage, the state covariance is sufficiently small compared to the measurement noise levels that the filter under-weights all new measurements. This is illustrated in Figure 3, which shows that the state estimate error remains effectively constant after two iterations. Henceforth, we refer as *apparent filter divergence*, or just filter divergence, to the situation in which a large error in the state estimate exists relative to a small state covariance matrix at steady state, which coincides with the definition used in references 4, 15.

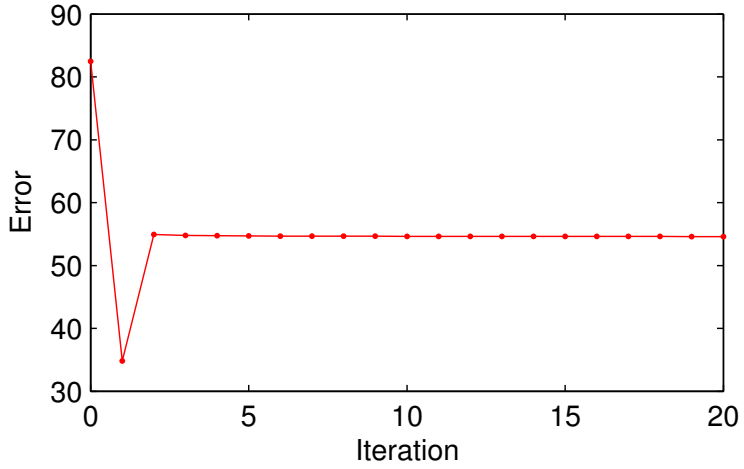

Figure 3. Variation of the EKF position error with filter iteration.

In summary, the example demonstrates that if the linear approximations of the measurement directions have a large dependence on the state estimate (i.e., $H(x) = \frac{\partial h(x)}{\partial x}$ is far from constant) and the measurements have very different noise levels, the linear update equations may lead the filter to diverge. To overcome the divergence of the EKF, both Plinval and Mandic investigated the possibility of artificially increasing the measurement noise levels to slow down the convergence process. This strategy will be referred to as bump-up EKF.

IV.A. Bump-up EKF strategies

A bump-up EKF strategy (B-EKF) tries to avoid the divergence of the filter by reducing the rate of convergence in the direction of the more accurate measurements, and "waits" for convergence in the less accurate directions. This strategy mitigates the over-reduction of the state covariance matrix. Additionally, the possible correlations in $P_{zz,k}$ due to a misinterpretation of the state covariance matrix will have a lower impact on the measurement update. The only difference in the formulae between these strategies and the EKF, is that a B-EKF will artificially increase the noise associated with the accurate measurements, and reduce this increment as a function of the confidence in current state vector estimates. Geometrically, this strategy means using larger and less eccentric confidence areas (or $P^{+}_{k,xx}$) compared to the EKF.

Based on this rationale, Plinval defined the following bump-up on the measurement noise level, which is assigned the label B-EKF 1:

$$\text{B-EKF 1:} \qquad R_{new} = R + H_k P^{-}_{xx,k} H^T_k \tag{13}$$

The right-hand side term $R + H_k P^{-}_{xx,k} H^T_k$ corresponds to the linear approximation of the measurement estimate covariance $P_{zz,k}$ (i.e., equation (11)) and the new measurement covariance is then $P_{zz,k,new} = R + 2H_k P_{xx,k} H^T_k$. Hence, the artificial increase is expected to be reduced as the state estimate uncertainty decreases. At steady state, this strategy is nearly equivalent to the EKF.

Figure 4 shows the norm of the estimation error $||\tilde{x}_{true} - \hat{x}_k||$ as a function of filter iteration k for B-EKF 1, EKF, and other filters (see below). The remarkable improvement of the B-EKF 1 with respect to the

EKF is consistent with reference 7. Mandic generalized this bump-up strategy and defined:

$$R_{new} = R + \alpha H_k P^-_{xx,k} H_k^T \tag{14}$$

where $\alpha \in \mathbb{R}^+$. This author noted that the α value of the bump-up and the magnitude of the error at steady state were related. It is further stated that the α value that minimizes the error at steady state seemed to depend on the error of the a priori information, and that no method for selecting α a priori was known.[8]

Further building on these strategies, we designed several alternative bump-up strategies to increase the state or measurement error noise covariance matrices (P or R). The rationale behind these new B-EKF is twofold; first, to reduce the probability of over-reduction of the state covariance matrix by artificially increasing the measurement noise levels; and second, to create a measurement noise matrix with a confidence area in the state space that is circle-shaped, thereby partially canceling possible misinterpretations of the correlations in P. The following bump-up strategies are labeled B-EKF 2, 3, and 4,

$$\text{B-EKF 2:} \qquad R_{new} = R + ||P^-_{xx,k}|| H_k H_k^T \tag{15}$$

$$\text{B-EKF 3:} \qquad R_{new} = ||J_k R J_k^T|| H_k H_k^T \tag{16}$$

$$\text{B-EKF 4:} \qquad P^-_{xx,k,new} = ||P^-_{xx,k}|| I_n \tag{17}$$

where J is the Jacobian of $h^{-1}(r,\theta)$ assuming the existence of this inverse function.

Equation (15) has the same form as (13), and becomes identical when $P^-_{xx,k}$ is a multiple of the identity. The usage of $||P^-_{xx,k}|| \cdot I_n$, instead of $P^-_{xx,k}$, is equivalent to considering the minimum circular area that contains the 1-σ confidence area defined by $P^-_{xx,k}$. Therefore, an error in the direction of the eigenvectors would have a minor impact. Figure 4 shows that the performance of B-EKF 1 and B-EKF 2 are very similar.

The bump-up method in equation (16) considers equivalent noise levels for different types of measurements and bump-up for only the lower accuracy terms of the R matrix in order to create similar convergence velocities in all directions. In the numerical simulation considered, starting from a state estimate $\hat{x}_0 = (20, 80)$ units means that a radial error of 1 unit is equivalent to an error of 1 unit along the radial direction, while an angular error of 1 degree is equivalent to an error of $\sim$1.4 units perpendicular to the radial direction. To compare the noise levels of different types of measurements, it is necessary to transform the measurement covariance matrix to the state space. Equation (16) uses a linear approximation, $J_k R J_k^T$, to apply such a transformation. In order to have comparable noises in the state space, this strategy uses $||J_k R J_k^T|| \cdot I_n$, and linearly transforms this covariance matrix back into the measurement space. The resulting R_{new} matrix, which is larger than R by construction, consists of comparable (in state space) noise levels for different types of measurements. Figure 4 shows that though the improvement relative to the EKF is significant, this bump-up performs worse than the previous B-EKF beyond the second iteration. Conceptually, the bump-up should affect all directions, not only the directions of the coarse measurements, thus effectively preventing over-reductions in any direction.

Equation (17) defines the only strategy that uses a bump-up of the state covariance $P^-_{xx,k}$ instead of the measurement covariance matrix R. It raises the lower accuracy terms of the state covariance matrix to impose a circularly shaped confidence area for the state estimate just before updating the state estimate with a new measurement. This minimizes the effect of a misinterpretation of the direction of the eigenvectors in the computation of $P_{zz,k}$, and $P_{xz,k}$. Figure 4 shows that this approach and the prior B-EKF provide similar performance for the current configuration. On a logarithmic scale, the improvement of the initial estimation using the bump-up strategies is approximately linear.

The main drawback of the B-EKF is that the speed of convergence, in terms of reducing the uncertainty associated to the state estimate, may decrease substantially with respect to the EKF.

V. Divergence process of the mtSOF

As previously introduced, the second-order filter is probably the best known among the high-order filters. These filters approximate the models by a second-order Taylor series expansion,[15] but the complexity and computational load required for an implementation of the full-scale second-order filter typically makes its implementation unfeasible, particularly in the vector case ($x \in \mathbb{R}^n, \quad n > 1$).[15] In the case of the second-order filter family, some simplifications have been designed to avoid the complexity of the full-scale implementation while retaining many of its useful properties. The version presented hereafter is referred to as the modified

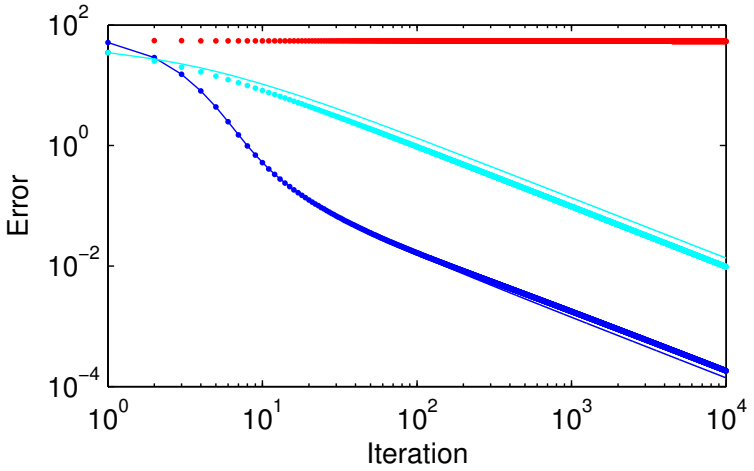

Figure 4. Variation of the position error for various bump-up strategies: (red) EKF, (blue dots) B-EKF 1, (blue line) B-EKF 2, (cyan line) B-EKF 3, and (cyan dots) B-EKF 4. Both axes are in logarithmic scale.

truncated second-order filter (mtSOF), which additionally assumes that the conditional density is nearly symmetric, and also that fourth and higher order even central moments can be neglected. The explicit update equations are:

$$\hat{z}_k = h(\hat{x}_k^-) + b_m \tag{18}$$

$$P_{zz,k} = R + H_k P_{xx,k}^- H_k^T - b_m b_m^T \tag{19}$$

$$P_{xz,k} = P_{xx,k}^- H_k^T \tag{20}$$

where $b_{m,i} = \frac{1}{2} tr\{\frac{\partial^2 h_i(\hat{x}_k^-)}{\partial x^2} P_{xx,k}^+\}$, and i denotes the index for the vector component of h. The expressions for $\hat{x}_k^+$, $P_{xx,k}^+$, and $P_{xz,k}$ are identical to equations (6), (7), and (12), respectively. Comparison of equations (10)–(11) and (18)–(19) shows that mtSOF is an EKF plus the b vector, which captures the second-order contribution of h.

Figure 5 shows the position error as a function of the filter iteration for the same experimental configuration presented in Section III. Comparison of Figures 5 and 3 shows that even though the mtSOF uses a second-order term b_m, any improvement over the EKF is marginal. Figure 5 also shows that mtSOF is very unstable. Inspection of the filter values reveals that the state covariance matrix does not retain its positive definite property after the first update. The $b_m b_m^T$ term causes a large reduction from $P_{xx,0}^+$ to $P_{zz,1}$ and, in turn, of $P_{xx,1}^+$. For this reason, the results of the filter in successive iterations become unrealistic and unpredictable. After a certain number of iterations, around 200, the filter reaches a steady state with an error of ∼40 units and a state covariance matrix corresponding to an uncertainty smaller than 0.04 square units in the angular direction, and 2E−7 units in the radial direction. These results indicate that the filter diverges because the state covariance matrix experiences an over-reduction right at the first iteration for the experiment being considered.

V.A. Bump-up mtSOF

We investigated a bump-up strategy of the measurement noise level similar to those designed for the EKF. We implemented the bump-up strategy defined in equation (13), which we will refer to as B-mtSOF for consistency, because of the good performance obtained with the B-EKF 1 and the reduced computational load associated with the bump-up. Figure 5 shows the estimation error for the mtSOF and the B-mtSOF. In this example, the B-mtSOF avoids the tendency of the state covariance matrix to lose its positive definiteness for more than 20 iterations and, therefore, shows a significant improvement over the mtSOF. However, the updated state covariance matrix loses positive definiteness after iteration 23, making the filter performance unpredictable. This leads to a sudden state estimate degradation near iteration 100.

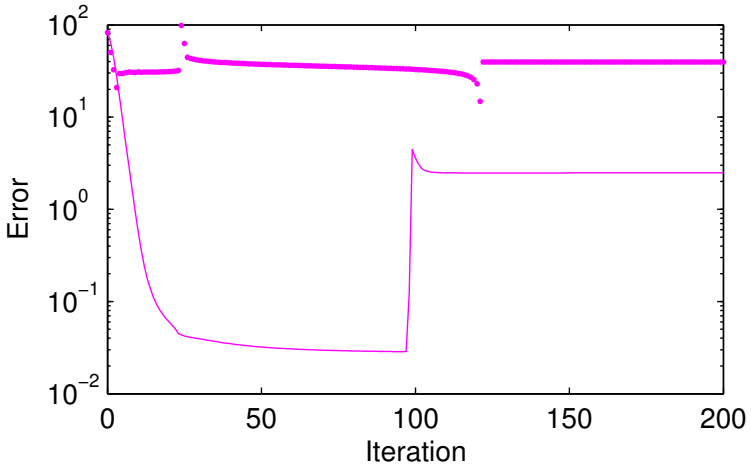

Figure 5. Variation of the state estimation error for the (dots) mtSOF and (continuous line) B-mtSOF.

VI. Divergence process of the UKF

The linear regression Kalman filters represent a set of EKF variants that approximate the state/measurement estimate and the associated uncertainty by a statistical linear regression through a well chosen set of points. This process allows multiple moments of the probability density function and terms of the Taylor approximation of the dynamic/measurement models to be considered. A representative example of this family is the UKF.[13,14,21] It requires the evaluation of the measurement model at several points, thereby avoiding the computation of the full Jacobian, in contrast with the EKF. This makes the UKF particularly well suited to the case where the evaluation of the Jacobian is complex or computationally expensive.

The explicit steps involved in updating the set of sigma points for this filter in absence of dynamics include the computation of:[5,12,22]

1. The sigma set from the predicted state and covariance matrix as

$$\mathcal{X}_k = \left[\begin{array}{ccc} \hat{x}_k^-, & \hat{x}_k^- + \gamma\sqrt{P_{xx,k}^-}, & \hat{x}_k^- - \gamma\sqrt{P_{xx,k}^-} \end{array} \right] \tag{21}$$

   where the matrix $\sqrt{P_{xx,k}^-}$ is interpreted as a set of n column vectors, and γ is a constant.

2. The measurements associated with this sigma set

$$\mathcal{Z}_k = h(\mathcal{X}_k) \tag{22}$$

$$\hat{z}_k = \sum_{i=0}^{2n} W_i^{(m)} \mathcal{Z}_{i,k} \tag{23}$$

   where $W_i^{(m)}$ and $W_i^{(c)}$ are a specific set of weights, m denotes mean, c denotes covariance, and i is the index of the sigma point (see reference [12] for additional details).

3. The expected correlations from the image set $\mathcal{Z}_k$ are

$$P_{zz,k} = R + \sum_{i=0}^{2n} W_i^{(c)} (\mathcal{Z}_{i,k} - \hat{z}_k)(\mathcal{Z}_{i,k} - \hat{z}_k)^T \tag{24}$$

$$P_{xz,k} = \sum_{i=0}^{2n} W_i^{(c)} (\mathcal{X}_{i,k} - \hat{x}_k^-)(\mathcal{Z}_{i,k} - \hat{z}_k^-)^T \tag{25}$$

$$\tag{26}$$

4. The update equations are the same as those used in the previous filters, i.e. equations (6)–(7).

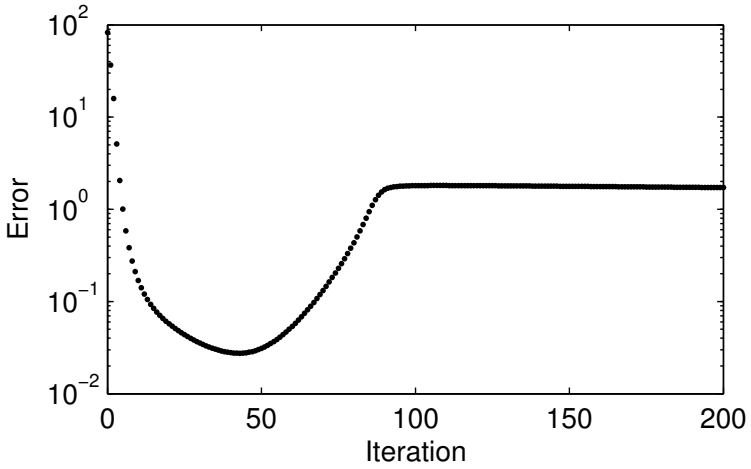

Figure 6. Variation of the state estimation error for the UKF.

Figure 6 shows the norm of the state estimation error as a function of filter iteration for the experimental configuration introduced in Section III. The error pattern of the estimated state of the UKF is counterintuitive because there is an initial phase of significant improvement (up to iteration ∼45), followed by a phase in which the error increases (between iterations ∼45–90), and a final phase where the improvement is marginal (beyond ∼90). Since the dynamic model of this example is static, the propagation equations cannot be the cause of this variation. To gain some insight into the relative accuracy of equations (10) and (23), Figure 7 shows the estimated measurement $\hat{z}_k$ after equations (10) and (23) for the UKF. This figure reveals that equation (23) is approximately four times more accurate than (10). This leads to an almost zero residual vector, and thus, a too small modification of the state estimate.

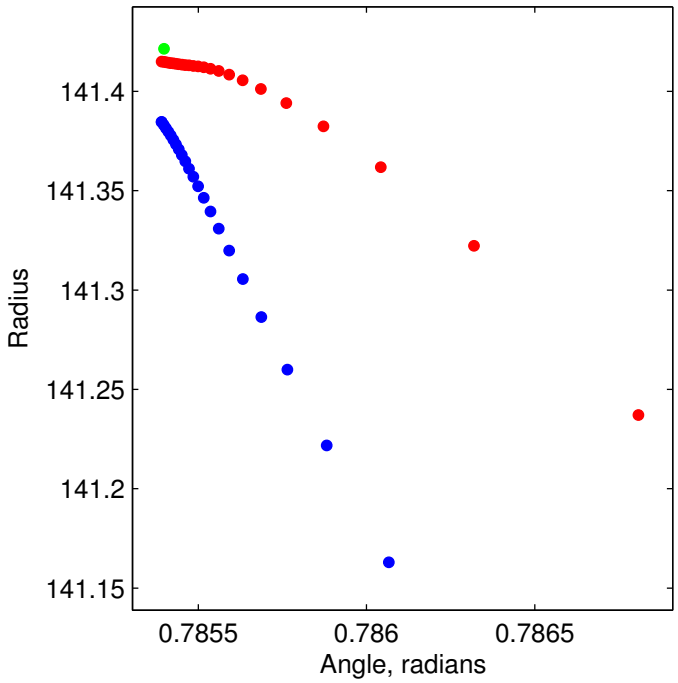

Figure 7. Measurement estimates $\hat{z}_k$ for the first 30 iterations using the (red) UKF equations and (blue) a linear approximation ($\hat{z}_k = h(\hat{x}_k^-)$). Within each curve, the time direction is from bottom-right to top-left. The true position $\tilde{z}_{true} = h(\tilde{x}_{true})$ is marked by a green dot.

The divergence process of the UKF can be summarized as follows:

1. At iteration number 14, the state estimate confidence area has contracted too much and the true

state $\tilde{x}_{true}$ falls outside the ellipsoid that approximates the confidence area $P_{xx,k}$ (see Figure 8(a) and 8(b)), as was the case when using the EKF with fewer iterates. Figure 8(c) shows the ellipsoid $P_{zz,k}$ that approximates the confidence area of the measurement estimate still includes the measurement corresponding to the true state $h(\tilde{x}_{true})$.

2. At iteration number 21, $h(\tilde{x}_{true})$ exits the ellipsoid defined by $P_{zz,k}$ (see Figure 8(d)).

3. Beginning at iteration number 29, the information from new measurements is misinterpreted by the filter and the state estimates begin moving away from the solution in the angular direction first, and then in the radial direction. The increasing condition number of $P_{xx,k}$ together with the discrepancy between the direction of the associated eigenvectors and the linear approximation of the measurements direction results in a significant correlation between radial and angular measurements in the P_{zz} matrix, as in the EKF example. This causes the residual information to be misinterpreted in the filter.

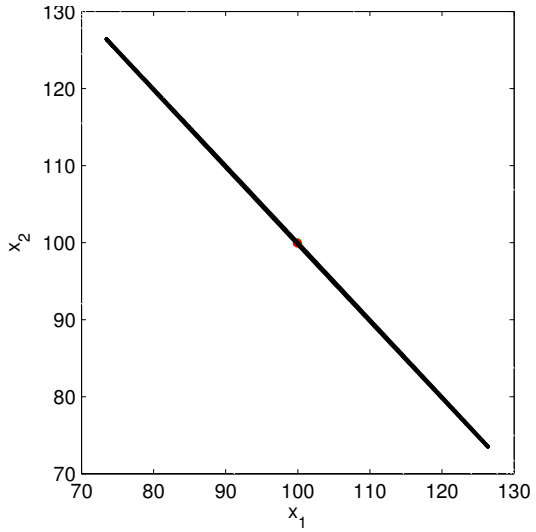

(a) (Black) 1-σ^2 confidence area for the (red) state estimate at iteration number 14.

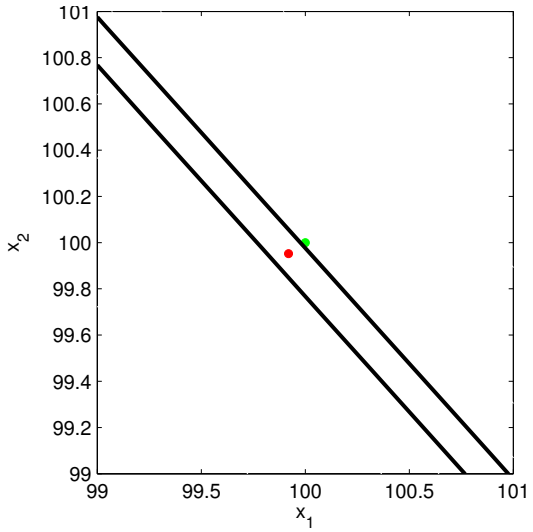

(b) Same as in Figure 8(a), zooming on x_{14}^{+}, and also showing (green) the true position $\tilde{x}_{true}$.

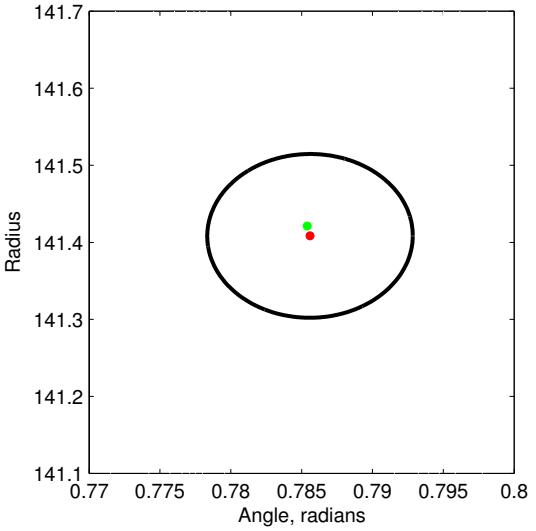

(c) (Black) 1-σ confidence area of the measurement variable z at iteration number 14. Red point corresponds to $\hat{z}_{14}$, and green point depicts $h(\tilde{x}_{true})$.

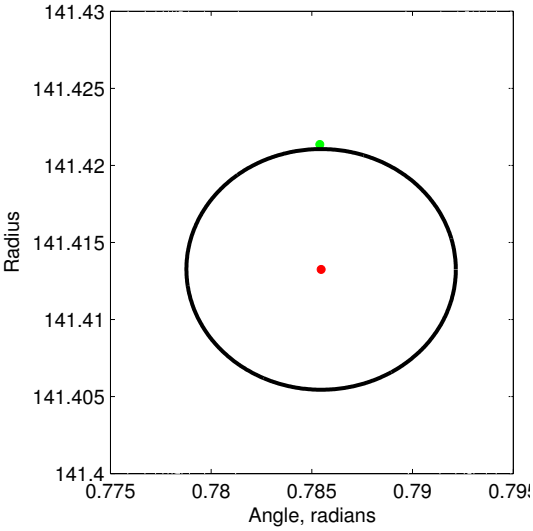

(d) Same as Figure 8(c) at iteration number 21.

Figure 8. Divergence process of the UKF.

In conclusion, the state covariance reduction appears to occur overly fast compared with the accuracy of the state estimates. The misalignment of the eigenvectors of $P_{xx,k}$, together with the high condition number of this matrix, leads the filter to a misinterpretation of new residuals. These two effects seem to lead the filter to ultimately diverge, as was described previously.

VI.A. Modifications to the UKF

Based on the hypothesis that the divergence of the UKF is due to the over-reduction of the covariance matrix compared to the error reduction in the state estimate, we defined two types of filter modifications, one by increasing the measurement noise level as in the B-EKF and B-mtSOF strategies, and second, by using more information from new measurements in the residuals. The first modification is labeled B-UKF and the second modification UKFz.

VI.A.1. B-UKF

Based on the results obtained examining bump-up strategies with the EKF, the bump-up UKF (B-UKF) is defined as follows

$$R_{new} = R + \sum_{i=0}^{2n} W_i^{(c)} (\mathcal{Z}_{i,k} - \hat{z}_k)(\mathcal{Z}_{i,k} - \hat{z}_k)^T$$

and

$$P_{zz,k,new} = R + 2\sum_{i=0}^{2n} W_i^{(c)} (\mathcal{Z}_{i,k} - \hat{z}_k)(\mathcal{Z}_{i,k} - \hat{z}_k)^T$$

Results using these modifications are presented in Figure 9 together with a comparison with the original UKF. This figure shows that the B-UKF has delayed the divergence of the nominal UKF, though it does not eliminate the problem.

VI.A.2. UKFz

The second modification alters the UKF algorithm by computing $\hat{z}_k$ as $h(\hat{x}_k^-)$ instead of using a high-order transformation. The rationale behind this approach is based on the results in Figure 7. That figure suggests that equation (23) is significantly more accurate than (10). For the same reason, the measurement residuals are smaller in the UKF than when using a linear approximation for the expected measurement computation. The residuals computed as $z_k - h(\hat{x}_k^-)$ are expected to point in a similar direction as the residual $z_k - \hat{z}_{k,ukf}$, but with a larger magnitude. Thus, $h(\hat{x}_k^-)$ should be nearly equivalent to an over-weighting of the new residuals in the state update equation, but without an increase in the contraction rate of the state covariance matrix. This strategy will be referred to as UKFz.

Figure 9 shows that the UKFz is the only approach that appears to avoid diverging at least for the experiment being considered. The convergence rate for this filter seems to be logarithmic (nearly linear in logarithmic scale), as was the case with the B-EKF strategies, though the UKFz is much faster. The figure shows that this filter reaches the numeric precision of the computer at the steady state very fast. Notice that the error at steady state is primarily due to the rounding errors associated to the computation of $\sqrt{P_{xx,k}^-}$.

VII. Sensitivity Analysis

The results presented in the previous sections were based on a representative experimental configuration, also used by several authors in the past, and a particular choice of model parameters such as the true position, relative noise level, and a priori measurement error and uncertainty.

We thus performed an extensive set of numerical simulations to examine the dependence of these results on variations of these choice parameters. As part of this sensitivity analysis, we assessed filter performance for the following and wide range of variations:

- Initial covariance error:

$$P_0 = \begin{pmatrix} \sigma^2 & 0 \\ 0 & \sigma^2 \end{pmatrix}, \qquad \text{where } \sigma \in [10^{-8}, 10^8]$$

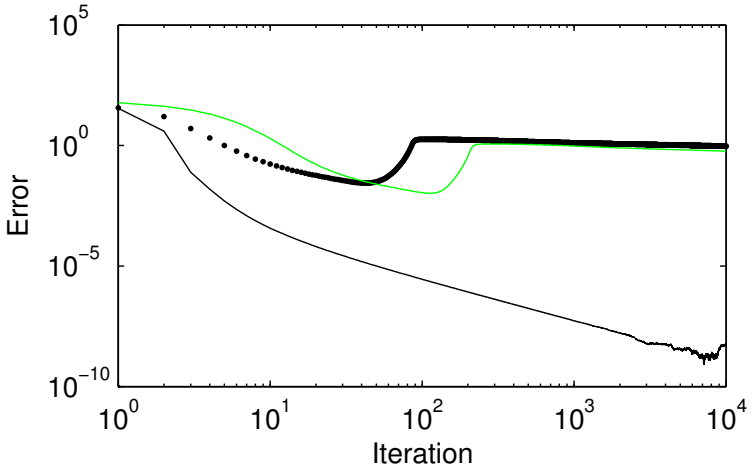

Figure 9. Variation of the state estimation error for the (black dots) UKF, (green line) the B-UKF, and (black line) the UKF-z strategies.

- Noise levels associated with different types of measurements:

$$R = \begin{pmatrix} 2.5\text{E-}5 + \beta & 0 \\ 0 & 6\text{E-}3 \end{pmatrix}, \qquad \text{where } \beta \in [0, 0.1]$$

- Error in the initial estimate ($= \hat{x}_0 - \tilde{x}_{true}$):

$$\hat{x}_0 = \tilde{x}_{true} + d \cdot (\cos\alpha, \sin\alpha)$$

  - for a fixed distance (angular variations): $\alpha \in [0, 2\pi), d = 82.4621$
  - for a fixed angle (distance variations): $\alpha \in \{0, \pi/4\}, d \in [10^{-11}, 10^4]$.

To be fully consistent with previous sections and enable direct comparison, the true position was always assumed to be at $\tilde{x}_{true} = (100, 100)$, the vehicle was static (i.e., $\dot{x} = f(t, x) = 0$), and there was no process noise ($Q \equiv 0$). This investigation does not include the effect of using different values for $\tilde{x}_{true}$ because this can be readily derived from the analysis of previous terms. A variation of the true state $\tilde{x}_{true} \neq (0, 0)$[a] is equivalent to a rotation and dilation of the state space. Therefore, the analysis of a variation on the true state can be derived from the analysis of a variation on the initial estimate and the covariance matrix magnitude.

We defined an indicator I of the filter performance to facilitate comparisons among the filters. It is defined as the ratio between the error at iteration number 1000, when the filters should have already reached steady state, and the initial error:

$$I = \frac{||\hat{x}_{1000} - \tilde{x}_{true}||}{||\hat{x}_0 - \tilde{x}_{true}||} \tag{27}$$

This parameter is thus an indicator of the error reduction, or improvement of the initial estimate, i.e., lower values of I correspond to larger improvements.

Figure 10 shows the improvement for the four types of analysis proposed above. Most of the filters (i.e., EKF, B-EKF 3 and 4, mtSOF, B-mtSOF, UKF, B-UKF) do not perform well regardless of the magnitude of the initial state covariance (see Figure 10(a)). The exception are filters B-EKF 1 and 2, and UKFz. In those cases, results suggest that it is important to start with a coherent P_0 covariance matrix to get good estimation performance (i.e., $\tilde{x}_{true}$ should be inside the 1-σ confidence area defined by $\hat{x}_0$ and P_0). If the initial covariance matrix is big enough, all three filters reach the computer numerical precision associated with the algorithm (the precision for the UKFz is worse than the B-EKF 1 and 2, primarily because of the computation of $\sqrt{P^-_{xx,k}}$). Otherwise, the filter is over-constrained and has no ability to improve the state estimate, as intended.

[a]The measurement model derivative does not exist at $(0, 0)$, and will be excluded from the configuration set for $\tilde{x}_{true}$.

Figure 10(b) shows the existing dependence on noise levels for several filters. For these filters, there appears to be a small interval of noise ratios in which filter performance is sensitive. The two noise levels can be considered comparable when $\sigma_{distance} \approx ||x|| \sin(\sigma_{angle})$. For the experiments performed $||x|| \approx 100$, and noises will be comparable when, $\sigma_{distance} \approx 100\ \sigma_{angle}$. When the noise levels on the angular measurements are larger ($\sigma_{distance} \ll 100\ \sigma_{angle}$), EKF, mtSOF, and UKF seem to diverge as in Sections V–VI. When the noise levels of the radial measurement are the largest ($\sigma_{distance} \gg 100\ \sigma_{angle}$), the state estimate uncertainty is much larger in the radial direction than in the angular direction. This situation reduces the convergence speed in the radial direction (vs. the speed in the angular direction). As a result, the orientation of the eigenvectors of the state covariance will vary little after a few iterations compared with the example in Section III. This indicates that when noise ratios are higher than ∼0.08, the UKF does not diverge. From this figure, the effect of the bump-up on the UKF is to reduce the impact of higher angle noise levels of the measurements. The same phenomenon occurs with the bump-up mtSOF when compared to the mtSOF. Performance of B-EKF, and UKFz strategies appear to be independent of the ratios between measurement noise levels.

Figure 10(c) shows that the performance of EKF, B-EKF 1-4, and UKFz vary as a function of the initial direction α. If $\hat{x}_0$ has the same angle as $\tilde{x}_{true}$, i.e. $\hat{x}_0 = \tilde{x}_{true} + (r \cdot \cos(\pm\pi/4), r \cdot \sin(\pm\pi/4))$, a filter only needs to improve the magnitude of the initial state, not the angle θ. This configuration ($\alpha = \pm\pi/4$), in fact, provides the best filter performance. The rest of the filters (mtSOF, B-mtSOF, UKF, and B-UKF) do not perform well regardless of the angle. In the case of the UKF, this fact highlights the high sensitivity of the filter on small variations of the measurement correlation matrix $P_{zz,k}$, that make the filter diverge even in the case that $\hat{x}_0$ and $\tilde{x}_0$ have the same angle (situation corresponding to $\alpha = \pm\pi/4$). In such a case, the small variations on the measurement correlation matrix are mainly due to the rounding errors in the computation of $\sqrt{P^-_{xx,k}}$.

In order to address the filter performance as a function of the initial distance r while being consistent with the conclusions regarding the analysis of the initial state covariance matrix, a different covariance matrix was considered for each initial state $\hat{x}_0 = \tilde{x}_{true} + (r \cdot \cos(\alpha), r \cdot \sin(\alpha))$. For each distance r, we chose $P = \sigma^2 I$, where $\sigma = 2.5r$, which guarantees that the true state is inside the initial confidence area. The performance curve of the filters in Figures 10(d) and 10(e) shows an unexpected pattern: when the initial estimate is close to the true state, the filter is unable to improve the initial error. This behavior is the subject of ongoing research.

VIII. Conclusions

We investigated the divergence problems of Kalman-type filters in the presence of nonlinearities for the EKF, high-order filters (mtSOF), and LRKF families (UKF). In particular, this work fully isolated the characteristics of the prediction and update phases of these filters and concentrated on the update phase by associating the nonlinearities exclusively to the measurement models. Measurements were modeled for two independent sensors with contrasting levels of accuracy. This type of investigation on sensor fusion is relevant for multi-satellite missions that rely on formation flying technologies.

It was determined that not only the EKF, but also the mtSOF and UKF may diverge, and that there is a common cause for the divergence of all these filters for the experimental confiuration considered. When using nonlinear measurement models, the accuracy of the state update equation is not commensurate with the reduction of the state covariance during the update phase. In the case of the EKF and UKF, the misalignment between the eigenvectors of the state covariance matrix is interpreted by the filter as a correlation between the measurements. This effect plays an important role in the divergence process.

We designed several modifications to these filters were proposed to circumvent the over-reduction of the state covariance without increasing the computational load over that of the baseline algorithms. The strategies were primarily based on a bump-up of the covariance matrix of the measurement noise. Those defined by equations (13) and (15) provided good performance when applied to the EKF, but did not eliminate divergence in the mtSOF and UKF. The accuracy of the measurement residuals or innovations was found to be key to the performance of the UKF. An additional modification was proposed to increase the importance of the residuals in the update phase (UKFz). This filter clearly outperforms all of the other filters investigated.

We performed a numerical study to examine the dependence of the filter performance on a priori filter information for key filter parameters such as $\hat{x}_0$, $P_{xx,0}$, and R. This study was intended to identify the set

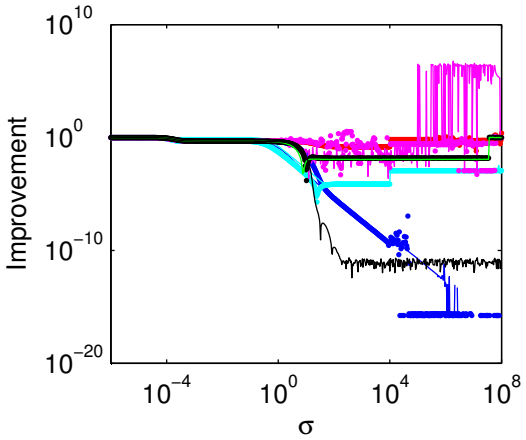

(a) Sensitivity on σ ($P = \sigma^2 I$). The initial error in distance is 82.46, therefore, σ should be larger than this value in order for the 1-σ confidence area to contain the true state.

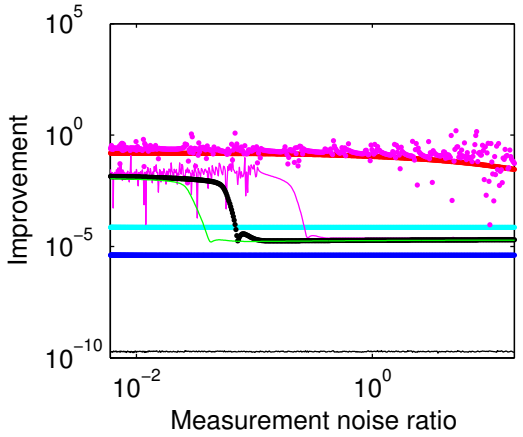

(b) Sensitivity on measurement noise levels ratio $\frac{\sigma_r}{\sigma_\theta}$.

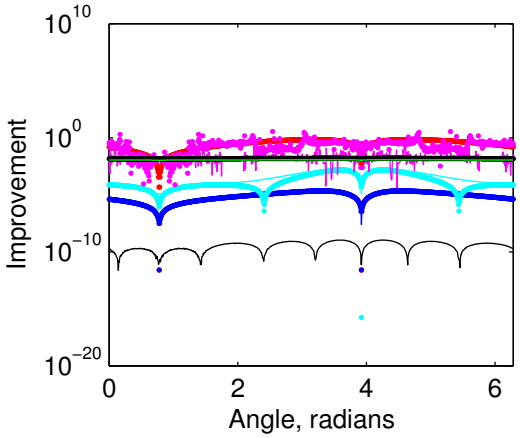

(c) Sensitivity on angle (α) variations.

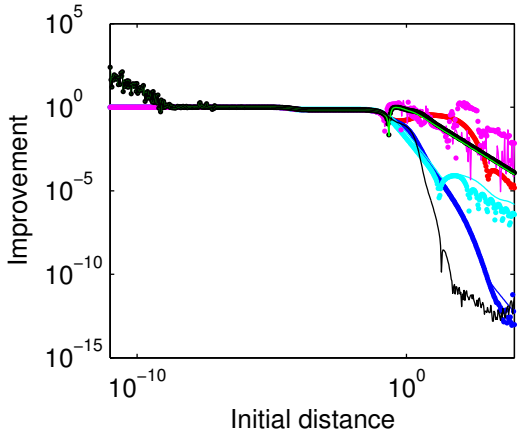

(d) Sensitivity to initial distance (d) in the horizontal direction ($\alpha = 0$).

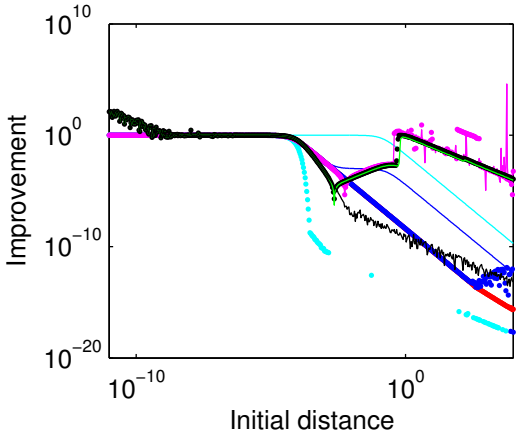

(e) Sensitivity to initial distance (d) in the same direction of x_0 ($\alpha = pi/4$).

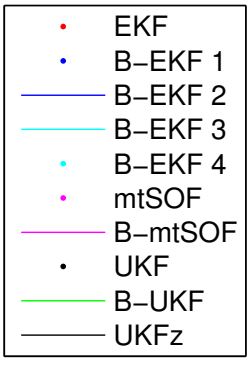

Figure 10. Variation of the state estimation error for various filters and experimental configurations.

of possible configurations that led previous filters to diverge, and to test the filters and filter modifications under a wide set of configurations. For most of the configurations tested, the divergence problems observed in the baseline experimental configuration remained. The filters that provide the best performance and that overcome the divergence problem were the B-EKF 1, B-EKF 2, and the UKFz. The UKFz was the fastest filter to reach steady-state and also showed excellent estimation performance.

IX. Acknowledgments

Discussion with Profs. Nicholas Roy (MIT) and Lena Valavani (Hellenic Space Systems) on Kalman-type filters were helpful in researching the divergence problem. Communications with Prof. James Davis (Center for Astrophysics) also helped improving the manuscript. This research was supported by a fellowship from the Spanish Ministry of Education and Science to perform a short-term visit at the Aeronautics and Astronautics Department at MIT.

References

[1]Borde, J., Teston, F., Santandrea, S., and Boulade, S., "Feasibility of the PROBA 3 formation flying demonstration mission as a pair of microsats in GTO," 55th International Astronautical Congress of the International Astronautical Federation, the International Academy of Astronautics, and the International Institute of Space Law, Oct. 2004.

[2]Geller, D., "Linear Covariance Techniques for Orbital Rendezvous Analysis and Autonomous Onboard Mission Planning," AIAA Journal of Guidance, Control and Dynamics, Vol. 29, No. 6, 2006, pp. 1404–1414.

[3]Scharf, D., Ploen, S., and Hadaegh, F., "A Survey of Spacecraft Formation Flying Guidance and Control (Part I): Guidance'," American Control Conference, 2003.

[4]Gelb, A., Applied Optimal Estimation, MIT Press, 1974.

[5]Ristic, B., Arulampalam, S., and Gordon, N., Beyond the Kalman filter: particle filters for tracking applications, Artech House, Boston, MA, 2004.

[6]Huxel, P. J. and Bishop, R. H., "Fusing inertial and relative range measurements for inertial navigation in the presence of large state error covariances," 16th AAS/AIAA Space Flight Mechanics Conference, 2006.

[7]Plinval, H., Analysis of Relative Navigation Architectures for Formation Flying Spacecraft, Master's thesis, Dept. of Aeronautics and Astronautics, Massachusetts Institute of Technology, Feb. 2006.

[8]Mandic, M., Distributed Estimation Architectures and Algorithms for Formation Flying Spacecraft, Master's thesis, Dept. of Aeronautics and Astronautics, Massachusetts Institute of Technology, June 2006.

[9]Brown, R. G. and Hwang, P. Y. C., Introduction to random signals and applied Kalman Filtering, John Wiley & Sons, 1992.

[10]Ferguson, P. and How, J., "Decentralized estimation algorithms for formation flying spacecraft," AIAA Guidance, Navigation and Control Conference, 2003.

[11]Bellaire, R. L., Kamen, E. W., and Zabin, S. M., "A new nonlinear iterated filter with applications to target tracking," SPIE Signal and Data Processing of Small Targets Conference, 1995, pp. 240–251.

[12]Haykin, S., The Unscented Kalman filter: Kalman filtering and neural networks, Wiley, 2001.

[13]Julier, S. and Uhlmann, J. K., "A New Extension of the Kalman Filter to Nonlinear Systems," 1999.

[14]Lefebvre, T., Bruyninckx, H., and Schutter, J. D., "Kalman filters for non-linear systems: a comparison of performance," International Journal of Control, Vol. 77, No. 7, 2004.

[15]Maybeck, P. S., Stochastic Models, Estimation and Control, New York, NY: Academy Press, 1982.

[16]Mitchell, M. L., CDGPS-Based Relative Navigation for Multiple Spacecraft, Master's thesis, Dept. of Aeronautics and Astronautics, Massachusetts Institute of Technology, June 2004.

[17]Nash, J. and Walker-Smith, M., Nonlinear Parameter Estimation an Integrated System in BASIC, New York: Marcel Dekke, 1987.

[18]der Merwe, R. V. and Wan, E., "The Square-Root Unscented Kalman Filter for State and Parameter Estimation," International Conference on Acoustics, Speech, and Signal Processing, 2001.

[19]Julier, S., Uhlmann, J., and Durrant-Whyte, H. F., "A new method for the nonlinear transformation of means and covariances in filters and estimators," Automatic Control, IEEE Transactions on, Vol. 45, No. 3, March 2000, pp. 477–482.

[20]Beichman, C., "The Terrestrial Planet Finder - The search for life-bearing planets around other stars," Astronomical Interferometry Meeting, 1998, pp. 719–723.

[21]Lefebvre, T., Bruyninckx, H., and Schuller, J. D., "Comment on "A new method for the nonlinear transformation of means and covariances in filters and estimators" [and authors' reply]," Automatic Control, IEEE Transactions on, Vol. 47, No. 8, Aug. 2002, pp. 1406–1409.

[22]Julier, S. and Uhlmann, J., "Unscented Filtering and Nonlinear Estimation," No. 3, IEEE, 2004.